Actin Filament Barbed-End Depolymerization by Combined Action of Profilin, Cofilin, and Twinfilin

Ankita Arya [1], Sandeep Choubey [2,3,*] and Shashank Shekhar [1,†]

[1] *Departments of Physics, Cell Biology and Biochemistry, Emory University, Atlanta, Georgia 30322, USA*

[2] *The Institute of Mathematical Sciences, Chennai 600113, India*

[3] *Homi Bhabha National Institute, Training School Complex, Anushaktinagar, Mumbai 400094, India*

(Received 8 June 2023; accepted 11 June 2024; published 16 July 2024)

Cellular actin dynamics results from the collective action of hundreds of regulatory proteins, majority of which target actin filaments at their barbed ends. Three key actin binding proteins—profilin, cofilin, and twinfilin—individually depolymerize filament barbed ends. Notwithstanding recent leaps in our understanding of their individual action, how they collectively regulate filament dynamics remains an open question. In the absence of direct and simultaneous visualization of these proteins at barbed ends, gaining mechanistic insights has been challenging. We have here investigated multicomponent dynamics of profilin, cofilin, and twinfilin using a hybrid approach that combines high-throughput single filament experiments with theory. We discovered that while twinfilin competes with profilin, it promotes binding of cofilin to filament sides. Interestingly, contrary to previous expectations, we found that profilin and cofilin can simultaneously bind the same filament barbed end, resulting in its accelerated depolymerization. Our study reveals that pairwise interactions can effectively capture depolymerization dynamics in simultaneous presence of all three proteins. We thus believe that our approach of employing a theory-experiment dialog can potentially help decipher multicomponent regulation of actin dynamics.

DOI: 10.1103/PRXLife.2.033002

I. INTRODUCTION

Cells regulate assembly and remodeling of their actin cytoskeleton in response to mechanochemical signals [1–3]. This response is mediated via the action of a large battery of proteins that combinatorially regulate dynamics of intracellular actin networks. The majority of these interactions take place at one of the two extremities of the actin filament, namely, the barbed end and the pointed end [1,4,5]. Decades of genetic experiments have identified key molecular components required for actin dynamics *in vivo*. Subsequent biochemical studies using purified proteins have since revealed how many of these components individually affect actin dynamics *in vitro*. Nonetheless, how cells integrate activities of these proteins to regulate actin assembly and disassembly remains poorly understood.

There are three dominant approaches for deciphering multicomponent regulation of actin dynamics. Classically, the bulk pyrene fluorescence assay has been the technique of choice for investigating actin dynamics [6]. The second approach involves direct visualization of fluorescently labeled protein molecules interacting with actin filaments using multicolor single-molecule microscopy. This technique has led to major discoveries, such as mechanism of filament branching [7,8], collaborative actin assembly by adenomatous polyposis coli (APC) and Spire [9], simultaneous association of elongators, blockers, and depolymerases with actin filament barbed end [10–13], and synergistic depolymerization of pointed ends by cofilin and cyclase associated protein [14–16]. Despite the great promise of this approach, labeling proteins without altering their activities and simultaneously visualizing multiple proteins is technically challenging and difficult to scale up. Furthermore, this approach is difficult to employ for transient associations ($\ll$1 s). The third approach is to leverage insights from structural studies of individual proteins bound to actin monomers (i.e., co-crystals) to predict how multiple proteins might simultaneously bind filaments and influence filament dynamics [10,17,18]. However, since most of these co-crystal structures are for proteins bound to G-actin, the majority of inferences are gained by docking structures of proteins bound to actin monomers on cryo-EM structures of actin filaments [10,18]. More recently, cryo-EM studies have allowed direct imaging of proteins bound to actin filament ends [19,20]. Nevertheless, this approach has so far only been successful for individual proteins bound to filament ends with a very high affinity. As a result, these structure-based methods only provide a static picture, taking into account only the long-lived binding configurations. Consequently, it has so far not been possible to employ this approach to investigate the effects of short-lived transient multiprotein complexes.

Here we combine high-throughput experimental measurements with theory to study multicomponent regulation of actin dynamics without the need to directly visualize the individual proteins. Fluorescence imaging of individual actin

*Contact author: sandeep@imsc.res.in

†Contact author: shekhar@emory.edu

filaments has been the technique of choice for visualizing dynamics of individual actin filaments for over three decades [21–23]. More recently, combining microfluidics and fluorescence imaging has enabled rapid and precise measurement of actin filament end dynamics across hundreds of filaments [10,14,15,24–32]. Such high-throughput quantitative measurements are amenable to theoretical modeling. To this end, falsifiable models predicated upon distinct mechanisms, which make specific predictions, can be built, and the corresponding predictions can be tested experimentally. To test the applicability of our theory-experiment approach, we asked how three key actin binding proteins—profilin, twinfilin, and cofilin—together cause barbed end depolymerization of actin filaments. Our results provide insights on whether these three proteins compete or cooperate at barbed ends to regulate filament depolymerization.

All three of these proteins can bind filamentous and monomeric actin. Their specific affinities and effects on barbed end dynamics, however, are highly sensitive to the nucleotide state of actin [1,3]. Actin filaments polymerize by adding ATP-actin subunits at their barbed ends. The newly assembled actin subunits rapidly hydrolyze their bound ATP, producing ADP-P_i actin filaments, and then release P_i at a much slower rate, producing ADP actin filaments [33,34]. Profilin preferentially binds ATP-G-actin subunits to inhibit filament nucleation, prevents monomer association at filament pointed ends [35–38], and supports processive elongation by delivering monomers to proline-rich proteins [formins, Ena/VASP (vasodilator-stimulated phosphoprotein) etc.] [39–41]. Cofilin and twinfilin, which are both members of the actin depolymerizing factor (ADF)/cofilin family of proteins, on the other hand bind aged ADP-actin monomers much more strongly than ATP-actin monomers [42–45]. More recently, each of these proteins has been shown to bind filament barbed ends and accelerate depolymerization of newly assembled ADP-P_i actin filaments [18,24,26,31]. Nevertheless, how these three proteins influence barbed end depolymerization when simultaneously present has never been addressed. We therefore applied our theory-experiment approach to investigate their combined interactions at ADP-P_i filament barbed ends. We have here elected to investigate the effects of these proteins on ADP-Pi rather than ADP-actin barbed ends to avoid complications due to cofilin's rapid severing of ADP-actin filaments.

To gain mechanistic insights on multiprotein regulation of actin depolymerization by these three proteins, we first considered two broad classes of mechanisms via which any two simultaneously present depolymerases can interact with filament barbed ends. In the first mechanism, the two proteins compete at barbed ends, resulting in their mutually exclusive binding where only one of them is bound (and depolymerizing barbed ends) at a given time. In the second mechanism, the two proteins simultaneously bind to the same barbed end, leading to increased rates of depolymerization. We developed an orthogonal approach by combining high-throughput experiments with theoretical modeling to distinguish between these two modes of multiprotein interactions. Using high-throughput microfluidics-assisted total internal reflection fluorescence (mf-TIRF) imaging of hundreds of actin filaments, we first carried out a careful examination of barbed end depolymerization by these depolymerases either individually or in pairs. Results from earlier studies suggest that profilin and cofilin bind actin monomers in a mutually exclusive fashion due to their targeting of the same barbed surface of G-actin [46–48]. However, we discovered that they are able to simultaneously associate with the same filament barbed end, leading to enhanced depolymerization. Surprisingly, when actin filaments were simultaneously exposed to a solution containing cofilin and twinfilin, we found that observed depolymerization rates were consistently lower than those predicted by a model accounting for simple competition between these two proteins for barbed end binding. Our analysis suggests that the presence of twinfilin at the barbed end might promote association of cofilin to filament sides. Interestingly, we discovered that pairwise interactions can successfully predict depolymerization dynamics in the simultaneous presence of all three proteins. Taken together, our results provide novel insights on simultaneous interactions of profilin, cofilin, and twinfilin with filament barbed ends using a promising approach combining theory and experiments. We believe this approach has far-reaching implications for elucidating underlying principles which govern multicomponent protein dynamics across a range of biological processes.

II. RESULTS

A. Quantitative characterization of effects of individual proteins on barbed end depolymerization

Previous studies have characterized the effects of profilin, cofilin, and twinfilin individually on barbed end depolymerization of ADP-P_i filaments [18,24,26,31]. To eliminate any inconsistencies due to use of different biochemical conditions and TIRF approaches among these studies, we first carried out a side-by-side quantitative characterization of each of these proteins using mf-TIRF [Figs. 1(a) and 1(b)]. Actin filaments were grown by exposing coverslip-anchored spectrin-actin seeds to a solution containing fluorescently labeled actin monomers and profilin [25] [Fig. 1(d)]. These filaments were all anchored at their pointed ends and their barbed ends remained free, thus allowing unambiguous recording of barbed end depolymerization of hundreds of filaments. Filaments were maintained in the ADP-P_i state throughout the experiment by supplementing the TIRF buffer with 50 mM P_i [26] (see Methods). Using this setup, we first measured the depolymerization rate of filament barbed ends in the presence of each of these depolymerases individually. Consistent with earlier studies, all three proteins increased barbed end depolymerization of ADP-P_i filaments in a concentration-dependent fashion [Figs. 1(f)–1(h)].

To understand this data, we employed a classical thermodynamic description of protein interactions to model actin filament depolymerization [see Fig. 1(a) of the Supplemental Material [49]]. A key assumption of this model is that the timescales associated with binding and unbinding of various depolymerases to actin barbed ends are much faster than the rate of depolymerization. In this model, a single protein molecule P binds to the barbed end of a bare actin filament. As a result, the barbed end can either be in a bare (free) state or a protein-bound state. Using statistical mechanics, we can

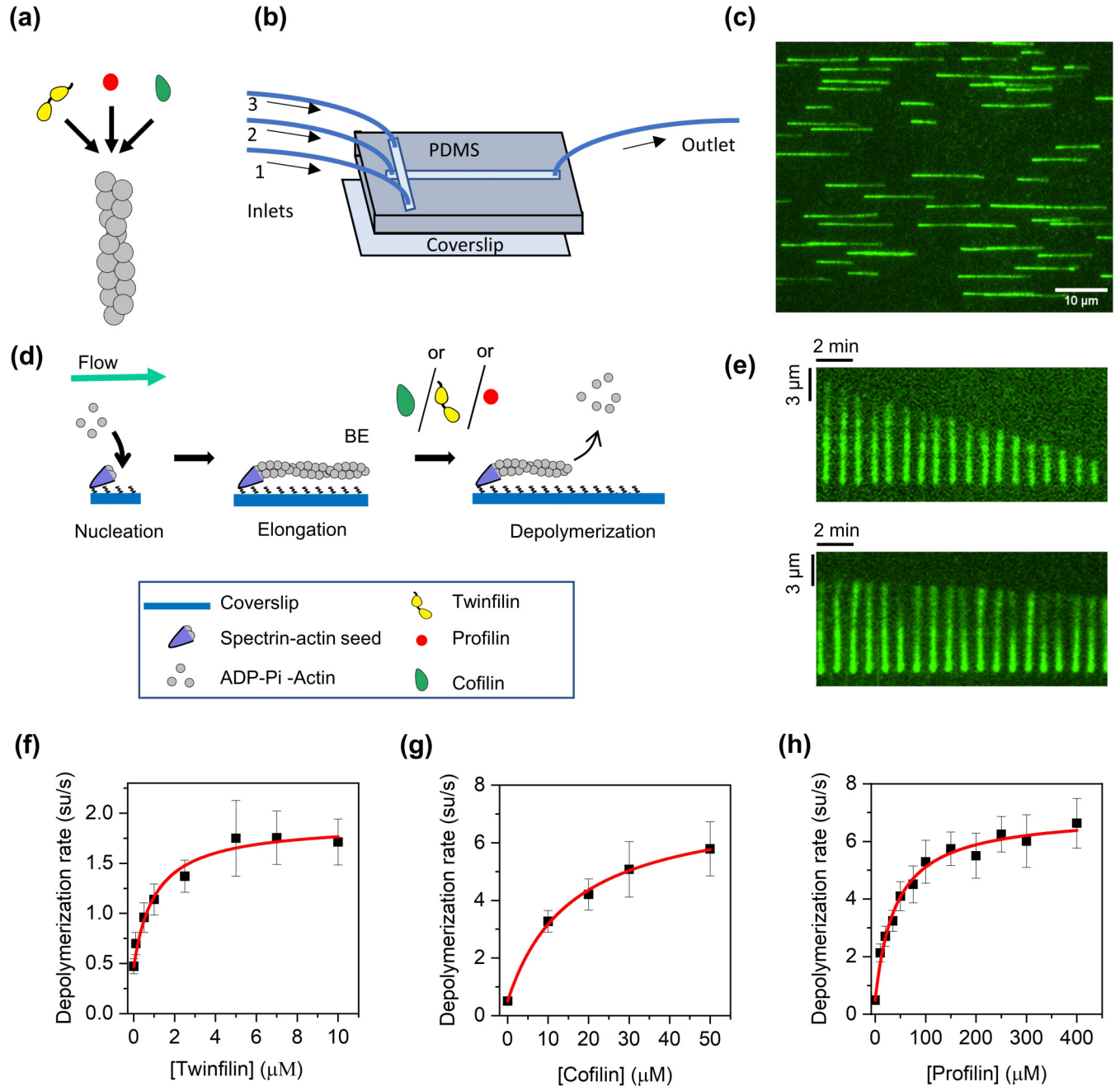

FIG. 1. Cofilin, profilin, and twinfilin individually accelerate depolymerization of ADP-P_i actin filament barbed ends. (a) Schematic representation of three depolymerases individually acting at the barbed end. (b) Schematic representation of the microfluidics setup. (c) An example of field of view of actin filaments in mf-TIRF microscopy. (d) Experimental strategy for measuring barbed end depolymerization of ADP-P_i filaments in the presence of cofilin, profilin, or twinfilin individually. Actin filaments with free barbed end were polymerized from coverslip-anchored spectrin-actin seeds by introducing 1 µM G-actin (15% Alexa-488 labeled) and 4 µM profilin in modified TIRF buffer. These filaments were then exposed to a flow containing cofilin, twinfilin, or profilin and the rate of depolymerization at their barbed ends (BE) was monitored. (e) Representative kymographs of Alexa-488-labeled actin filament (green) depolymerizing in absence (buffer, control) (top) and in presence of 100 µM profilin (bottom). (f) Rates (mean ± SD) of barbed end depolymerization as a function of mTwf1 concentration. Number of filaments analyzed for each concentration (left to right): 62, 64, 62, 59, 67, 62, 64, and 67. A fit (line) of a simple kinetic model of depolymerization to the data is shown [see Eq. (2) and Supplemental Material [49]). (g) Rate (mean ± SD) of barbed end depolymerization as a function of cofilin concentration. Number of filaments analyzed for each concentration (left to right): 51, 144, 142, 136, and 79. A fit to the model is shown (see Supplemental Material [49]). (h) Rates (mean ± SD) of barbed end depolymerization as a function of cofilin concentration. Number of filaments analyzed for each concentration (left to right): 66, 79, 79, 73, 72, 56, 82, 93, 98, 87, 72, and 63. A fit to the model is shown (see Supplemental Material [49]). Parameters K_D and d_1 were determined from the fit. All experiments were performed three times and yielded similar results. The data and the fit shown are from a single trial. Here, su/s refers to subunits/s.

TABLE I. Barbed end depolymerization rates and dissociation constants for twinfilin, profilin, and cofilin obtained by fitting Eq. (2) to experimental data pooled from three independent trials (see Fig. 2 of the Supplemental Material [49]). Note that Figs. 1(f)–1(h) show representative data from a single trial. K_D is the dissociation constant and d_1 is the depolymerization rate when twinfilin, profilin, or cofilin are bound to the barbed end.

Protein	K_D (μM)	d_1 (su/s)
Twinfilin	0.77 ± 0.32	1.93 ± 0.18
Profilin	18.7 ± 4.8	6.6 ± 0.4
Cofilin	19 ± 6	8.3 ± 1.0

obtain the equilibrium weights of these two states, respectively [49], which are dictated by the protein's dissociation constant ($K_{D,P}$) and its concentration (C_P) in the solution. Rates of depolymerization in each of these states are given by d_0 and d_1, respectively. The average depolymerization rate (D_P) of a filament can then be written as

$$D_P = d_0 p_0 + d_1 p_1, \tag{1}$$

where p_0 is the probability of the filament end being in the bare state and p_1 is the probability of the filament end being in the protein-bound state (see the Supplemental Material [49] for details). After a bit of algebra, the depolymerization rate can be rewritten as

$$D_P = \frac{d_0 K_{D,P} + d_1 C_P}{C_P + K_{D,P}}. \tag{2}$$

We use Eq. (2) to compare our model to experimental data. Our model fits the experimental data well [Figs. 1(f)–1(h)] and allows extraction of depolymerization rates in the bare state (d_0), protein-bound state (d_1), and dissociation constant ($K_{D,P}$) for each of these proteins separately (see Table I below for fitted parameters). The rate of depolymerization from the bare barbed end is given by $d_0 = 0.50 \pm 0.08$ subunits per second (su/s) [mean ± standard deviation (SD)], obtained after pooling experimental data from different days. As expected from our model, the experimentally observed depolymerization rates increased with the bulk concentration and eventually saturated. At saturating concentration, the barbed end is almost always occupied by a protein molecule. The quantitative characterization carried out in this section paves the way for studying the combined effects of multiple proteins on barbed end depolymerization.

B. Uncovering multiprotein barbed end depolymerization using competitive and simultaneous binding models

We have thus far quantified the effects of individual proteins. In living cells, however, multiple proteins simultaneously regulate actin dynamics. Proteins targeting the same site on a filament can bind either competitively (i.e., mutually exclusively) or simultaneously. We developed two broad classes of thermodynamic models to discriminate between these two possible modes of interaction, i.e., competitive or simultaneous binding. In the competitive binding model, two proteins bind the barbed end in a mutually exclusive manner, whereby only one of them occupies the barbed end at a given moment. In contrast, in the simultaneous binding model, two proteins can simultaneously occupy the same barbed end. Below, we discuss the two models in greater detail.

When two proteins A and B bind the barbed end competitively (following the competitive binding model), the barbed end can exist in three different states—free, protein A bound, or protein B bound—as shown in Fig. 2(a). The statistical weights of these different states in equilibrium are governed by the dissociation constants of the two proteins and their concentrations, respectively [50]. Each of these three states is characterized by its distinct depolymerization rate—d_0 (free), $d_{1,A}$ (protein A bound), and $d_{1,B}$ (protein B bound). Switching between these states results in an average depolymerization rate given by

$$D_{AB} = \frac{d_0 K_{D,A} K_{D,B} + d_{1,A} C_A K_{D,B} + d_{1,B} C_B K_{D,A}}{K_{D,A} K_{D,B} + C_A K_{D,B} + C_B K_{D,A}}, \tag{3}$$

where C_A and C_B are concentrations of the two proteins, and $K_{D,A/B}$ is the dissociation constant of protein A or B at the barbed end (see the Supplemental Material [49] for details). The competitive binding model exhibits a complex concentration-dependent behavior, as shown in Fig. 2(c). At low concentrations, the average depolymerization rate in simultaneous presence of both the proteins is higher than when either of the proteins is present alone. In contrast, at higher concentrations the average depolymerization rate with two proteins present lies somewhere in between the depolymerization rates of individual proteins.

Next, we considered the second class of model, namely, the simultaneous binding model [Fig. 2(b)]. In contrast to the competitive binding model, the simultaneous binding model can lead to an additional barbed end state when the two proteins A and B are both simultaneously bound to the barbed end. Consequently, the barbed end can now exist in four distinct states: free, protein A bound, protein B bound, or both proteins A and B bound. The rates of depolymerization from these different states are given by d_0 (free), $d_{1,A}$ (protein A bound), $d_{1,B}$ (protein B bound), and $d_{2,AB}$ (both proteins A and B simultaneously bound). The average depolymerization for this model is given by

$$D_{AB} = \frac{d_0 K_{D,A} K_{D,B} + d_{1,A} C_A K_{D,B} + d_{1,B} C_B K_{D,A} + d_{2,AB} C_A C_B}{K_{D,A} K_{D,B} + C_A K_{D,B} + C_B K_{D,A} + C_A C_B}, \tag{4}$$

where C_A and C_B are concentrations of the two proteins, and $K_{D,A/B}$ is the dissociation constant of proteins A or B at the barbed end. A key assumption of our model is that the dissociation constants of either of the proteins remain unaffected by the presence of the other protein. The simultaneous binding model predicts that the average depolymerization rate in the presence of both proteins will either be additive or superadditive as compared to the individual depolymerization rates of proteins as shown in Fig. 2(d).

Overall, the competitive and cooperating models make distinct falsifiable predictions that can be tested experimentally and allow us to extract mechanistic insights into multicomponent depolymerization of actin, as we demonstrate in the ensuing sections.

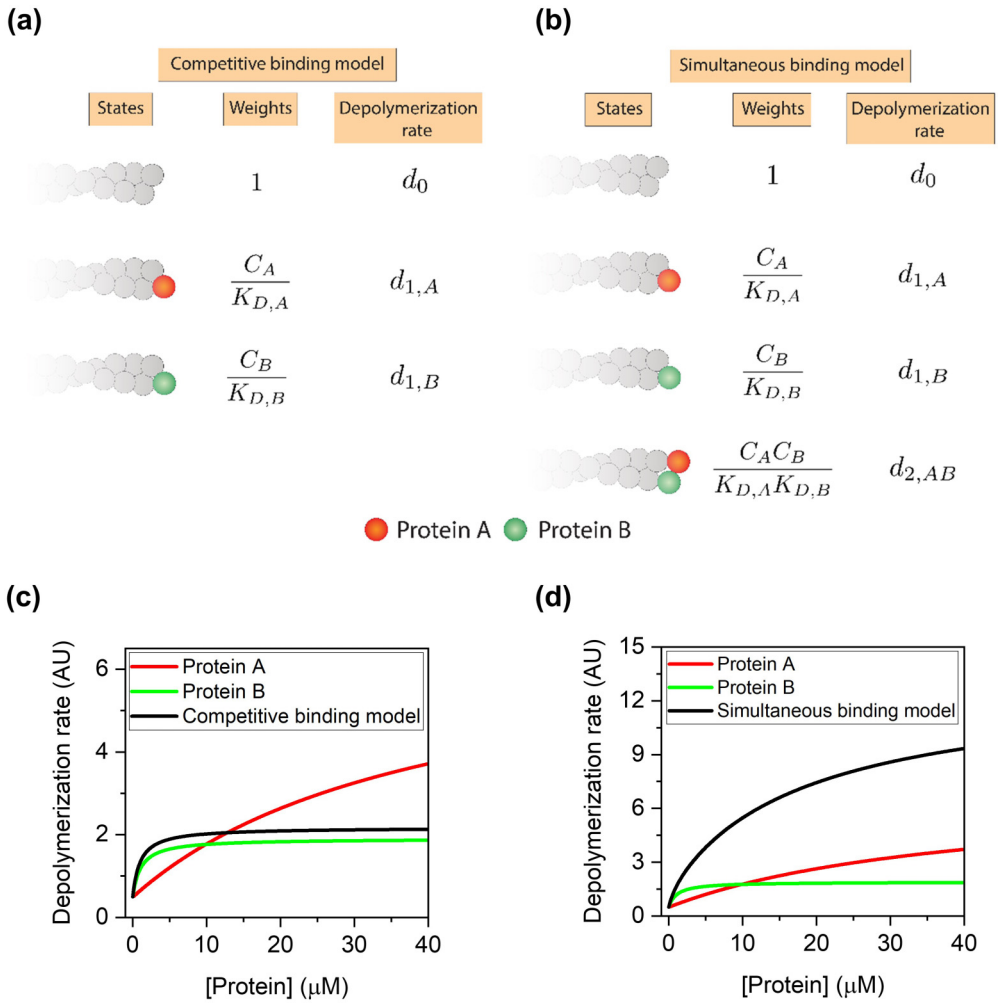

FIG. 2. (a) Thermodynamic model for competitive interaction of two proteins at the barbed end. At equilibrium, each of the microstates has a corresponding statistical weight [50]. These weights are governed by concentration ($C_{A,B}$) and dissociation constant ($K_{D,A/B}$) of the proteins. The rates of depolymerization from the three states are d_0 (free), $d_{1,A}$ (protein A bound), and $d_{1,B}$ (protein B bound), respectively. (b) Thermodynamic model for simultaneous interaction of two proteins at the barbed end. Each of the microstates has a corresponding equilibrium statistical weight [50]. These weights are governed by concentration ($C_{A,B}$) and dissociation constant ($K_{D,A/B}$) of the proteins. The rates of depolymerization from the four states are d_0 (free), $d_{1,A}$ (protein A bound), $d_{1,B}$ (protein B bound), and $d_{2,AB}$ (both protein A and B simultaneously bound). (c) Average rate of barbed end depolymerization (D_{AB}) in the presence of A alone (red), B alone (green), and A and B together (black) as a function of their concentration for competitive binding model (see Supplemental Material [49]). (d) Average rate of barbed end depolymerization (D_{AB}) in the presence of A alone (red), B alone (green), and A and B together (black) as a function of their concentrations for the simultaneous binding model (see Supplemental Material [49]). In (c) and (d) the x axis is the concentration of the proteins, either alone or together. When both are present together, their concentrations are the same.

C. Profilin and twinfilin bind competitively to filament barbed ends

We first asked how profilin and twinfilin together depolymerize actin filament barbed ends. X-ray diffraction structural studies indicate that twinfilin and profilin both bind to the barbed surface of actin monomers [46,48,51]. Based on this, we hypothesized that these proteins bind in a mutually exclusive manner to filament barbed ends as well.

Similar to earlier experiments, free barbed ends of ADP-P_i actin filaments were exposed to a solution containing both profilin (human profilin-1) and twinfilin (mouse twinfilin-1) [Fig. 3(a)]. We first systematically tuned the concentration of twinfilin while keeping profilin's concentration fixed and compared the recorded depolymerization rates with that of twinfilin alone. In the absence of profilin, increasing concentrations of twinfilin led to a monotonic increase followed by a saturation at high concentrations (∼5 μM). In sharp contrast, the addition of profilin qualitatively altered the depolymerization behavior; increasing concentrations of twinfilin (in the presence of profilin) caused a monotonic decrease [Fig. 3(b)]. These depolymerization rates were then compared to predictions from our competitive binding model using Eq. (3) (see the Supplemental Material [49]). The model prediction matched the experimental data well, thereby validating our hypothesis that profilin and twinfilin bind to the filament barbed end in a mutually competitive manner [Fig. 3(b)].

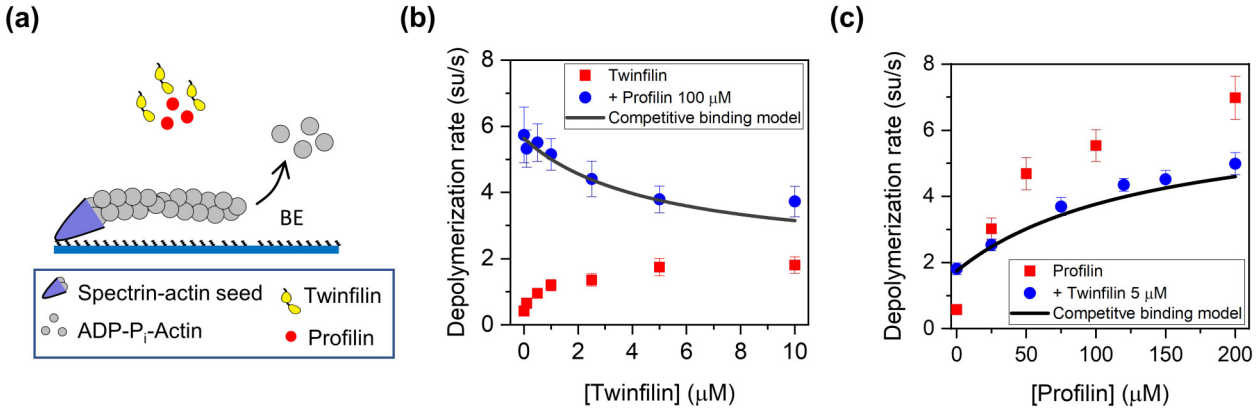

FIG. 3. Profilin and twinfilin bind filament barbed ends competitively. (a) Schematic depiction of the experimental strategy for measuring barbed end depolymerization of ADP-P_i actin filaments in the simultaneous presence of twinfilin and profilin. Actin filaments with free barbed ends were polymerized from coverslip-anchored spectrin-actin seeds by introducing 1 μM G-actin (15% Alexa-488 labeled) and 4 μM profilin in modified TIRF buffer containing 50 mM P_i. These filaments were then exposed to a flow containing twinfilin and profilin, and their rate of barbed end (BE) depolymerization was monitored. (b) Rates (mean ± SD) of barbed end depolymerization in the presence of a range of concentrations of twinfilin alone (red symbols) or additionally supplemented with 100 μM profilin (blue symbols). Number of filaments analyzed for each concentration of twinfilin (red curve, left to right): 67, 54, 55, 52, 26, 37, and 42. Number of filaments analyzed for 100 μM profilin and twinfilin (blue curve, left to right): 63, 65, 64, 65, 63, 58, and 61. The experimental data were compared to predictions from the competitive binding model of depolymerization (black curve) (see Supplemental Material [49]). (c) Rate (mean ± SD) of barbed end depolymerization in the presence of a range of concentrations of profilin alone (red symbols) or additionally supplemented with 5 μM twinfilin (blue symbols). Number of filaments analyzed for each concentration of profilin (red symbols, left to right): 32, 38, 61, 50, and 61. Number of filaments analyzed for 5 μM twinfilin and profilin (blue symbols): 60 for each concentration. The experimental data were compared to predictions from a competitive binding model of depolymerization (black curve) (see Fig. 3 of the Supplemental Material [49]). Model predictions were made using d_0 for free barbed ends, and K_D and d_1 for twinfilin-bound or profilin-bound barbed ends. The values used here were extracted from single-protein data in Figs. 1(g) and 1(h) (also see Table I).

Notably, these model predictions are robust to uncertainties in the input parameter values (see Fig. 3 of the Supplemental Material [49]). To further validate the competitive binding model, we systematically varied the concentration of profilin, keeping twinfilin concentration fixed [Fig. 3(c)]. We found that the experimental data were once again consistent with the predictions of the competitive binding model. Interestingly, as profilin concentration was tuned, the presence of twinfilin did not alter the qualitative behavior of the observed rate of depolymerization. However, quantitatively, the observed depolymerization rate in the presence of both proteins always remained lower than that of profilin alone.

D. Profilin and cofilin can simultaneously occupy the same filament barbed end

After validating profilin and twinfilin's competitive binding to barbed ends, we decided to investigate how cofilin and profilin together impact barbed end depolymerization. Since twinfilin and cofilin belong to the same protein family, we hypothesized that they would bind the filament barbed end similarly. Therefore, we expected that, similar to twinfilin, cofilin would also compete with profilin in a mutually exclusive fashion for the filament barbed ends. Indeed, earlier studies have shown that they both bind the barbed surface on actin monomers, thereby indicating that they might bind filament barbed ends competitively [46–48,52]. However, it remains to be determined whether these proteins also compete at the barbed ends of actin filaments. To this end, we decided to experimentally characterize filament depolymerization rates in the presence of these two proteins and then challenge the experimental results against predictions of our competitive binding model.

We exposed free barbed ends of ADP-P_i actin filaments to a solution containing either profilin and cofilin alone or together [Fig. 4(a)]. Keeping the concentration of profilin fixed, we first tuned the concentration of cofilin and compared the recorded depolymerization rates with that of cofilin alone [Fig. 4(b)]. In the absence of profilin, increasing concentrations of cofilin led to a monotonic increase in depolymerization rate. However, the addition of profilin led to an overall increase in average depolymerization rates with increasing concentrations of cofilin.

We then compared these experimental findings with predictions from our competitive binding model [Eq. (3)]. Contrary to our expectation, the competitive binding model failed to capture the experimental data, thereby falsifying our hypothesis that profilin and cofilin bind filament ends mutually exclusively [Fig. 4(b)]. The experimentally measured average depolymerization rates were consistently greater than the depolymerization rates predicted by the competitive model across the probed concentration range. A similar behavior was observed when cofilin concentration was kept constant and profilin concentration was varied [Fig 4(c)].

We suspected the possibility of simultaneous binding of profilin and cofilin at the barbed end, which could potentially lead to such high experimentally observed depolymerization rates. To test this possibility, we employed the simultaneous binding model [Eq. (4)], as defined in the earlier section. Unlike the competitive binding model where the filament barbed end could exist in three distinct states, namely, free, profilin

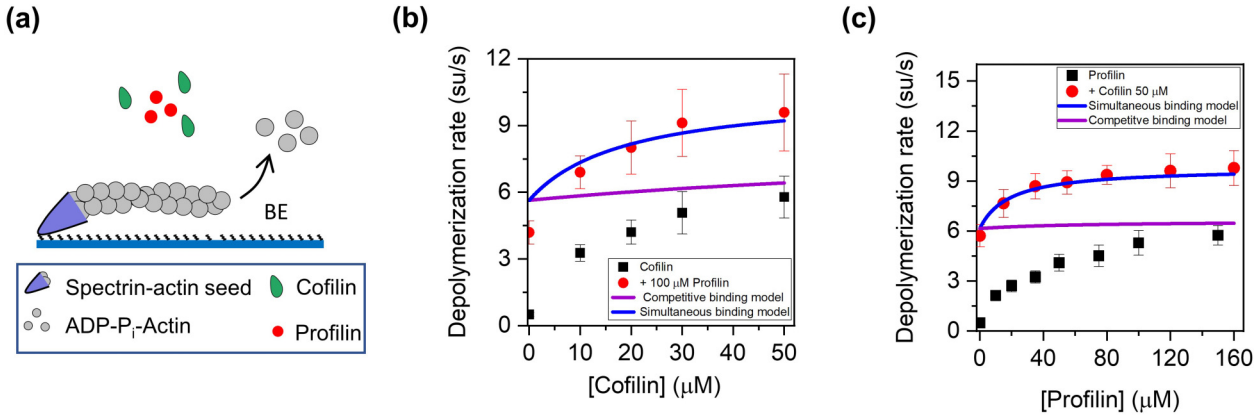

FIG. 4. The competitive binding model fails to explain the simultaneous interaction of profilin and cofilin with barbed ends. (a) Schematic representation of the experimental strategy for measuring barbed end depolymerization of ADP-P_i actin filaments in the presence of cofilin and profilin. Actin filaments with free barbed end were polymerized from coverslip-anchored spectrin-actin seeds by introducing 1 μM G-actin (15% Alexa-488 labeled) and 4 μM profilin in modified TIRF buffer containing 50 mM P_i. These filaments were then exposed to a flow containing cofilin and profilin, and the rate of depolymerization at their barbed ends (BE) was monitored. (b) Rates (mean ± SD) of barbed end depolymerization in the presence of cofilin alone (black symbols) or in the presence of 100 μM profilin (red symbols). Number of filaments analyzed for each concentration of cofilin (black symbols, left to right): 51, 144, 142, 136, and 79. Number of filaments analyzed for 100 μM profilin and cofilin (blue symbols, left to right): 106, 129, 151, 104, and 91. The experimental data were compared to predictions from the competitive model (purple). Model predictions were made using d_0 for free barbed ends, and K_D and d_1 for twinfilin-bound or profilin-bound barbed ends. The values used here were extracted from single-protein data in Figs. 1(g) and 1(h) (also see Table I). To compare the data against simultaneous (blue) binding model, we fit the data to our model. We kept the following parameters fixed: d_0 for free barbed ends, K_D and d_1 for profilin-bound or cofilin-bound barbed ends. d_4 was the only free parameter that we extracted from the fit (see the Supplemental Material [49]). (c) Rates (mean ± SD) of barbed end depolymerization for ADP-P_i filaments in the presence of profilin alone (black symbols) or in the presence of 50 μM cofilin (red symbols). Number of filaments analyzed for each concentration of profilin (black symbols, left to right): 66, 79, 79, 73, 72, 56, 82, and 93. Number of filaments analyzed for 50 μM cofilin and profilin (red symbols, left to right): 58, 63, 60, 60, 60, 61, and 92. The experimental data were compared to predictions from competitive (purple) and simultaneous (blue) binding models (see the Supplemental Material [49] and Supplemental Fig. 4).

bound, and cofilin bound, the simultaneous binding model entails an additional fourth state where both cofilin and profilin are simultaneously bound to the barbed end. This fourth state is characterized by its own distinct depolymerization rate. *A priori*, this rate cannot be determined from experiments characterizing the depolymerization rates of individual proteins [Figs. 1(d)–1(f)]. Hence, in order to test this model, we treated the depolymerization rate from the fourth state as a free parameter in our model. By tuning this depolymerization rate, we found that the simultaneous binding model indeed captured the experimentally measured depolymerization rates [Figs. 4(b) and 4(c)]. Interestingly, this theory-experiment dialog demonstrates that profilin and cofilin can occupy the barbed end simultaneously. Moreover, when present together, the resulting depolymerization rate is higher than that of individual proteins. In summary, we showed that cofilin and profilin can simultaneously occupy the actin filament barbed end, thereby enhancing the rate of depolymerization.

E. Barbed end bound twinfilin promotes association of cofilin

After validating that while profilin competes with twinfilin and it can simultaneously occupy the same barbed end with cofilin, we then asked how cofilin and twinfilin together impact barbed end depolymerization. Since twinfilin and cofilin both contain ADF homology domains, we hypothesized that these proteins would bind filament barbed ends in a mutually exclusive manner. To test this hypothesis, we measured barbed end depolymerization of ADP-P_i filaments in the presence of these two proteins. Keeping the concentration of twinfilin fixed, we tuned the concentration of cofilin and compared the recorded depolymerization rates with that of cofilin alone [Figs. 5(a) and 5(b)]. In the absence of twinfilin, increasing concentrations of cofilin led to a monotonic increase in depolymerization rate. In sharp contrast, the addition of twinfilin qualitatively altered the depolymerization behavior; increasing concentrations of cofilin (in the presence of twinfilin) caused a monotonic decrease. The simultaneous presence of cofilin and twinfilin led to a significant reduction in the rate of depolymerization to values below 1 su/s [Fig. 5(b)]. A similar behavior was observed when twinfilin concentration was kept constant and cofilin concentration was varied [Fig. 5(c)]. A systematic comparison between experimental data with predictions from the competitive binding model falsified our hypothesis (see Fig. 5(a) of the Supplemental Material [49]). Notably, while the model predicted an increase in average depolymerization rate as a function of cofilin concentration (at fixed twinfilin concentration), the experimental data showed the exact opposite trend. Next, we considered the possibility of twinfilin and cofilin simultaneously occupying the barbed end (see Fig. 5(b) of the Supplemental Material [49]). This model also failed to explain the data. Taken together, we find that the experimental observations are inconsistent with both of our simple

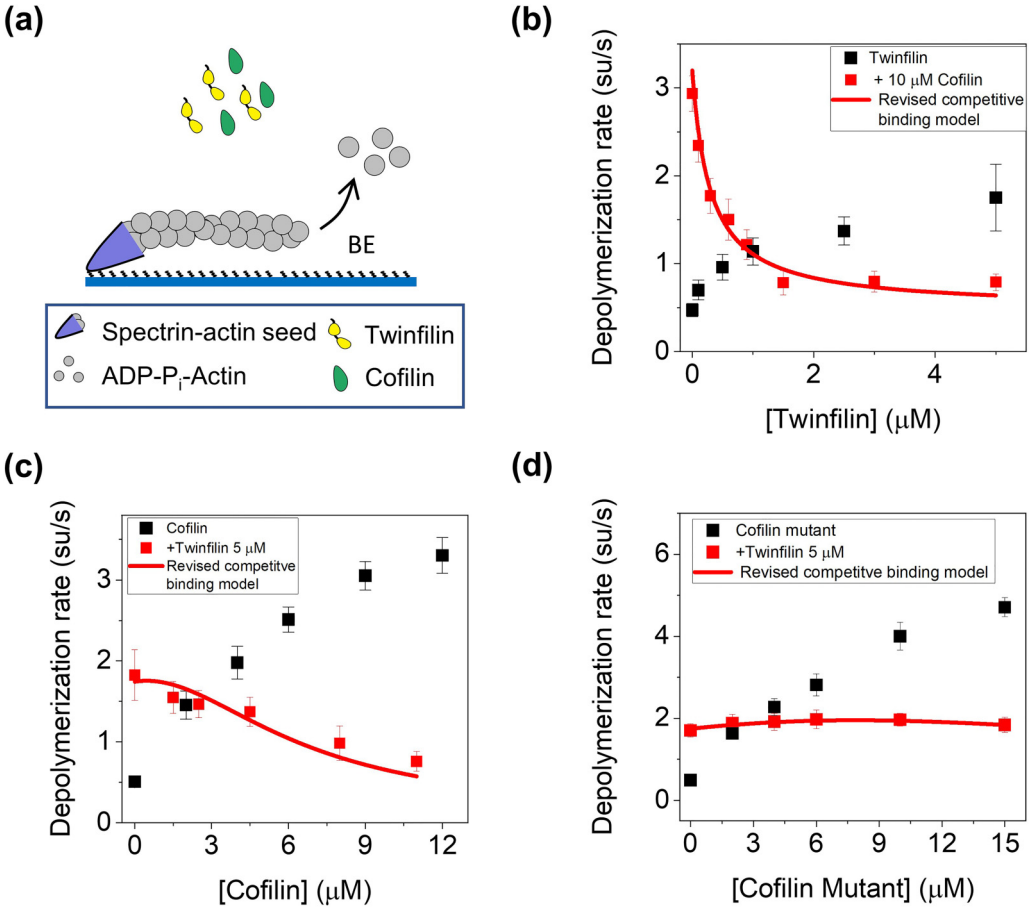

FIG. 5. Twinfilin and cofilin bind filament barbed ends competitively. (a) Schematic depiction of the experimental strategy for measuring barbed end depolymerization of ADP-P_i actin filaments in the presence of twinfilin and cofilin. Actin filaments with free barbed ends were polymerized from coverslip-anchored spectrin-actin seeds by introducing 1 μM G-actin (15% Alexa-488 labeled) and 4 μM profilin in modified TIRF buffer containing 50 mM P_i. These filaments were then exposed to a flow containing twinfilin and cofilin, and the rate of depolymerization at their barbed ends (BE) was monitored. (b) Rates (mean ± SD) of barbed end depolymerization in the presence of twinfilin alone (black symbols) or additionally supplemented with 10 μM cofilin (red symbols). Number of filaments analyzed for each concentration of twinfilin (black symbols, left to right): 62, 64, 62, 59, 67, and 62. Number of filaments analyzed for twinfilin and 10 μM cofilin (red symbols, left to right): 61, 62, 52, 63, 60, 45, 50, and 59. The experimental data were fit to the revised competitive (red) model (Eq. (3); see Supplemental Material [49]). Parameters d_0 for free barbed ends, and K_D and d_1 for twinfilin-bound or cofilin-bound barbed ends were kept fixed and their values were extracted from single-protein data in Figs. 1(g) and 1(h) (also see Table I). The parameter $K_{D,SC} = 181$ μM was taken from a previous study [55]. ω was the only free parameter which we extracted from the fit as 1084.1. (c) Rates (mean ± SD) of barbed end depolymerization in the presence of cofilin alone (black symbols) or additionally supplemented with 5 μM twinfilin (red symbols). Number of filaments analyzed for each concentration of cofilin (black symbols, left to right): 40, 60, 60, 60, 60, 60, and 60. Number of filaments analyzed for 5 μM twinfilin and cofilin (red symbols, left to right): 50, 51, 37, 63, 42, and 38. The experimental data were compared to predictions (red thick line) from the revised competitive model (Eq. (3); see Supplemental Material [49]). Predictions were made using d_0 for free barbed ends, and K_D and d_1 for twinfilin-bound or profilin-bound barbed ends. Their values were extracted from single-protein data in Figs. 1(g) and 1(h) (also see Table I). The parameter $K_{D,SC} = 181$ μM was taken from a previous study [55], and $\omega = 1084.1$. (d) Rates (mean ± SD) of barbed end depolymerization in the presence of K96A D98A mutant of cofilin-1 alone (black symbols) or additionally supplemented with 5 μM twinfilin (red symbols). Number of filaments analyzed for each concentration of cofilin (black symbols): 60. Number of filaments analyzed for 5 μM twinfilin and mutant cofilin (red symbols, left to right): 60, 60, 61, 60, 60, and 60. The experimental data were compared to predictions (red thick line) from the revised competitive model (Eq. (3); see the Supplemental Material [49], and Supplemental Fig. 5). Parameters d_0, K_D, d_1, and ω were kept fixed as in (c); $K_{D,SC}$ for the mutant was taken as 724 μM, fourfold lower than the wild-type protein.

single-site barbed end binding models (see Figs. 5(a) and 5(b) of the Supplemental Material [49]). This implies that barbed end interactions of these two proteins (when simultaneously present) might be more complex.

A recent study showed that binding of cofilin to the sides of ADP-actin filaments leads to a dramatic reduction in barbed end depolymerization to rates lower than in control reactions [31]. Although side binding of cofilin has so far mainly been studied in the context of ADP-actin filaments, acceleration of phosphate release by cofilin suggests that it can also interact (albeit weakly) with sides of ADP-P_i actin filaments [53,54]. We therefore asked if considering side binding of cofilin in addition to barbed end binding can explain our experimental findings. Since we did not observe a reduction in barbed

end depolymerization even at high cofilin concentrations (Fig. 1), we wondered if the added presence of twinfilin might stabilize the weak interactions of cofilin with sides of ADP-P_i actin filaments, thereby reducing the depolymerization rate.

Taking into account these possibilities, we expanded our barbed end competitive model to include side binding of cofilin, aided by the barbed end presence of twinfilin. Specifically, we considered side binding of one cofilin molecule per actin protofilament (near the barbed end). In this revised competitive model, we used the cofilin side-binding dissociation constant $K_{D,SC} = 181\,\mu M$ for newly assembled actin filaments (i.e., ADP-P_i-F-actin) as determined in a previous single-molecule study [55] and kept ω, the cooperativity between side binding of cofilin and barbed end bound twinfilin, as a free parameter (see Fig. 1(b) of the Supplemental Material [49]). To test this model, we fit it to our experimental data, where we varied twinfilin at fixed cofilin concentration [Fig. 5(b)]. We found that this model captured experimental data well and allowed us to infer the free parameter ω as 1084.1. Using the inferred parameter, we predicted the effect of varying cofilin concentration at fixed twinfilin concentration [Fig. 5(c)]. The average depolymerization rate as predicted by the model matches the data well, thereby suggesting a possibility of side binding of cofilin influencing twinfilin's interaction with barbed ends.

To further validate our revised competitive model, we employed a cofilin mutant (K96A D98A) which exhibits a fourfold lower affinity for filament sides [31,56]. Although both the wild-type and mutant exhibited similar qualitative concentration-dependent behavior, the mutant exhibited a slightly faster maximal depolymerization and higher dissociation constant ($d_1 = 14.4 \pm 1.4\,su/s$, $K_{D,P} = 31.5 \pm 5.5\,\mu M$) when compared to wild-type cofilin ($d_1 = 8.3 \pm 1.0\,su/s$, $K_{D,P} = 19 \pm 6\,\mu M$) [Fig. 5(d)]. Surprisingly, the model predicted that, upon varying mutant cofilin concentration at a fixed twinfilin concentration, the average depolymerization rate would remain largely unaltered. We tested this model by systematically comparing its predictions with experimental data and found that the predictions matched our data extremely well [Fig. 5(d)]. Taken together, we have uncovered a potentially new mechanism in which the presence of twinfilin at the filament barbed end promotes the association of cofilin to filament sides which results in a dramatic reduction of barbed end depolymerization.

F. Pairwise interactions are sufficient to explain three-protein interactions

Following pairwise investigation of profilin, cofilin, and twinfilin, we asked if we could leverage our learnings from their pairwise interactions to predict depolymerization dynamics of the barbed end when all three proteins were present simultaneously (Fig. 6). To this end, we constructed a model for the three-protein case by combining their pairwise interactions (see Fig. 1(c) of the Supplemental Material [49]). This model makes specific predictions for the average depolymerization rate in the presence of all three proteins. In particular, we made two sets of predictions. First, we varied twinfilin concentration in the presence of fixed concentration of profilin and cofilin. To our surprise, our model predicted a steeper drop in depolymerization rates upon addition of cofilin in comparison to when only twinfilin and profilin were present [Fig. 6(b)]. Second, we varied cofilin concentration in the presence of fixed concentration of twinfilin and profilin. Once again, our model predicted a much steeper drop in average depolymerization upon addition of profilin in comparison to when only cofilin and twinfilin were present [Fig. 6(c)]. We put these predictions to test using experiments. We find excellent agreement between the predictions and our experimental measurements. Taken together, our results show that pairwise interactions alone are sufficient to predict multicomponent depolymerization dynamics resulting from three proteins.

III. DISCUSSION

A large array of proteins interact with actin filaments to facilitate intracellular actin assembly and remodeling [1]. Majority of these interactions occur at the barbed end of the actin filament [4]. As a result, these proteins can either bind filament barbed ends in a mutually exclusive manner or simultaneously associate with filament barbed ends. However, directly visualizing multiple proteins simultaneously interacting with the barbed end is technically challenging. Here we have presented an alternate approach that combines experimental measurements with predictive theoretical modeling to fill this gap. We show that high-throughput measurements coupled with theory can help uncover features of multicomponent dynamics that would otherwise remain intractable. We believe our approach is especially useful when studying multicomponent dynamics of proteins that bind filament very transiently ($\ll 1\,s$), as directly visualizing these short-lived interactions using classical methods like multicolor single-molecule imaging is not possible.

In particular, we looked at three proteins—profilin, cofilin, and twinfilin—all of which individually depolymerize barbed ends of newly assembled (ADP-P_i) actin filaments. To dissect how they simultaneously regulate actin depolymerization, we experimentally measured their effects individually, in pairs and all together, and then challenged these measurements against predictions of our theoretical models.

Cofilin and profilin compete for binding actin monomers [47]. We therefore hypothesized that the two proteins would also bind filament barbed ends in a mutually exclusive manner. To our surprise, we found that cofilin and profilin can simultaneously occupy filament barbed ends. Our analysis showed that the competitive binding model failed to explain the experimentally observed depolymerization rates when both cofilin and profilin are present. We instead found that the simultaneous binding model captured the experimentally observed depolymerization rates and, therefore, supports the alternative possibility that cofilin and profilin can simultaneously occupy the actin filament barbed end [Fig. 6(d)]. How can we explain the simultaneous binding of these two proteins to filament barbed ends from a structural perspective? F-actin subunits have long been thought to adopt a flattened conformation compared to a G-actin subunit. A recent cryo-EM study, however, revealed that while this holds for subunits in the bulk of the filament, the W loop and the C terminus of the

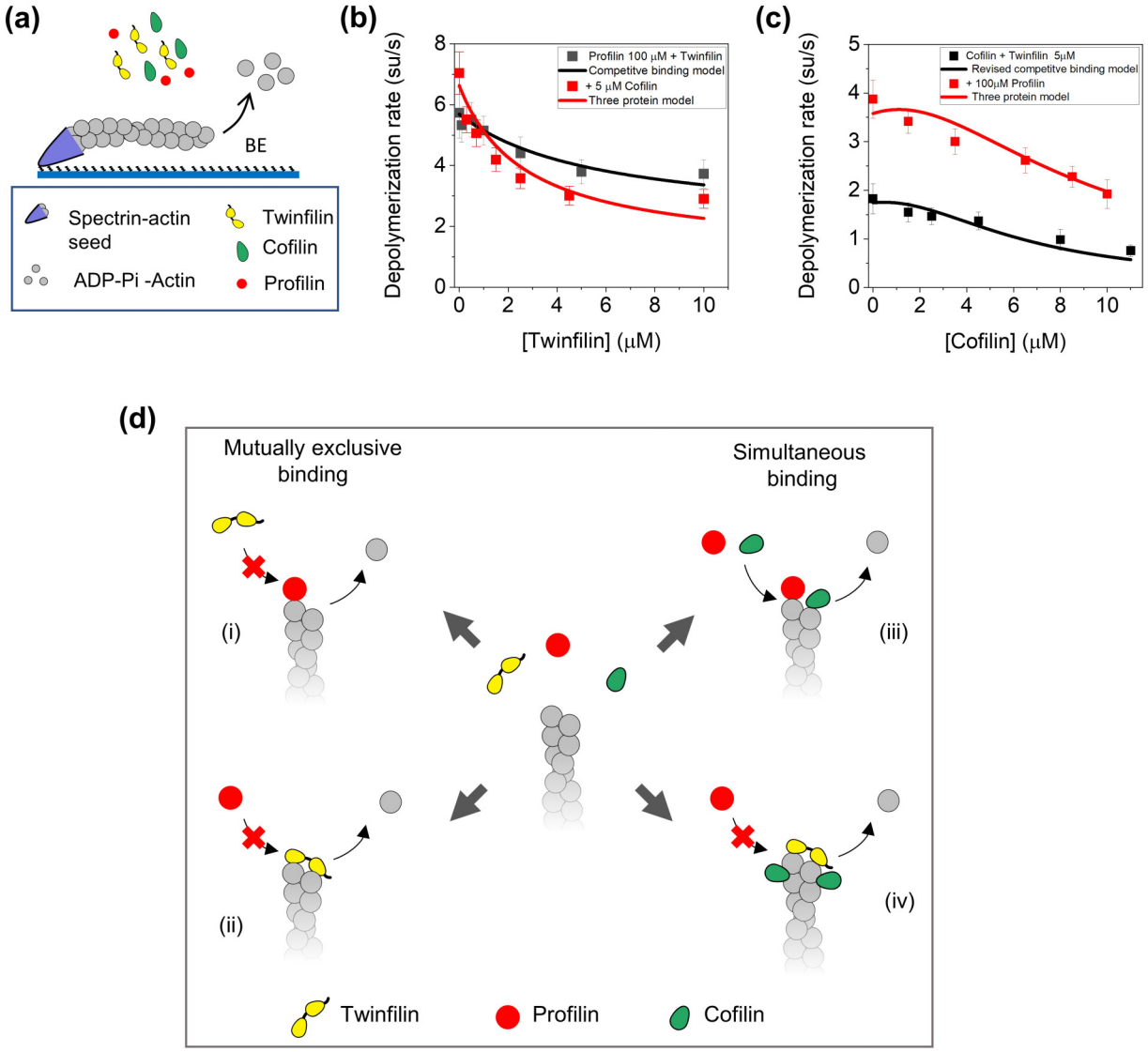

FIG. 6. Three-protein model based on pairwise interactions fails to explain depolymerization dynamics in presence of profilin, twinfilin, and cofilin. (a) Schematic representation of the experimental strategy for measuring barbed end depolymerization of ADP-P_i actin filaments in the presence of profilin, twinfilin, and cofilin. Actin filaments with free barbed ends were polymerized from coverslip-anchored spectrin-actin seeds by introducing 1 μM G-actin (15% Alexa-488 labeled) and 4 μM profilin in modified TIRF buffer containing 50 mM P_i. These filaments were then exposed to a flow containing profilin, twinfilin, and cofilin and the rate of depolymerization at their barbed ends (BE) was monitored. (b) Rates (mean ± SD) of barbed end depolymerization in the presence of 100 μM profilin and twinfilin (black symbols) or additionally supplemented with 5 μM cofilin (red symbols). Number of filaments analyzed for each concentration of 100 μM profilin and twinfilin (black symbols, left to right): 63, 65, 64, 65, 63, and 58. Number of filaments analyzed for 100 μM profilin, 5 μM cofilin, and twinfilin (red symbols, left to right): 66, 60, 61, 62, 61, 61, and 63. The experimental data were compared to predictions from the two-protein competitive (black) binding model for 100 μM profilin and twinfilin and the three-protein model (red) for 100 μM profilin, 5 μM cofilin, and twinfilin (see Supplemental Material [49]). (c) Rates (mean ± SD) of barbed end depolymerization in the presence of 5 μM twinfilin and cofilin (black symbols) or additionally supplemented with 100 μM profilin (red symbols). Number of filaments analyzed for each concentration of 5 μM twinfilin and cofilin (black symbols, left to right): 50, 51, 37, 63, 42, and 38. Number of filaments analyzed for 5 μM twinfilin, 100 μM profilin, and cofilin (red symbols, left to right): 60, 62, 62, 60, 61, and 62. The experimental data were compared to predictions from the two-protein revised competitive (black) model for 5 μM twinfilin and cofilin and the three-protein model (red) for 5 μM twinfilin, 100 μM profilin, and cofilin (see the Supplemental Material [49], and Supplemental Fig. 6). For both (b) and (c), predictions were made using d_0 for free barbed ends, and K_D and d_1 for twinfilin-bound, profilin-bound, or cofilin-bound barbed ends. Their values were extracted from single-protein data in Figs. 1(g) and 1(h) (also see Table I). The parameter $K_{D,SC} = 181$ μM was taken from a previous study [55], and $\omega = 1084.1$. (d) Working model for multicomponent interactions of profilin (red), twinfilin (yellow), and cofilin (green) at the actin filament barbed end. While profilin and twinfilin bind barbed ends in a mutually exclusive manner (i), (ii), profilin and cofilin can simultaneously occupy a filament barbed end (iii). Side binding of cofilin to the terminal actin subunits can aid barbed end binding of twinfilin (iv).

terminal barbed end actin subunit's hydrophobic cleft exhibit a conformation akin to G-actin [20]. This revelation offers a structural rationale for understanding how monomer-binding proteins profilin and cofilin might also be able to interact with filament barbed ends. We used co-crystal structures of human profilin bound to G-actin [48] and an ADF homology domain bound to G-actin [46]. Both of these were docked on the two terminal F-actin subunits of the cryo-EM structure of an ADP-P_i actin filament [57]. In agreement with Courtemanche and Pollard [18], we found that while profilin can bind the terminal actin subunit (n) with minimal clashes, it clashes directly with the terminal actin subunit (n) when docked on the penultimate subunit ($n-1$) (see Fig. 8 of the Supplemental Material [49]). This suggests that profilin's interactions with the filament barbed end might originate solely from its interaction with the terminal barbed end subunit. Upon docking the ADF homology domain on the actin filament, however, we found that it could comfortably interact with both the terminal and penultimate actin subunits (n and $n-1$) at the barbed end (see Fig. 9 of the Supplemental Material [49]). Taken together, our structural analysis suggests that the most likely explanation for our findings is that profilin binds to the terminal actin subunit and cofilin preferentially to the penultimate one, thus providing a pathway for them to be able to occupy the filament barbed end simultaneously (see Fig. 10 of the Supplemental Material [49]). As a result, the simultaneous presence of profilin and cofilin destabilizes both the subunits at the barbed end, causing the fastest ever depolymerization rates measured for ADP-P_i barbed ends [Figs. 4(b) and 4(c)].

Since twinfilin and cofilin are both members of the ADF/cofilin family of proteins, twinfilin would also be expected to simultaneously bind barbed ends with profilin. Surprisingly, our analysis showed that, unlike cofilin and profilin, twinfilin and profilin bind barbed ends in a mutually exclusive manner [Fig. 6(d)]. While twinfilin contains two connected ADF homology domains connected via a short peptide linker, cofilin only contains a single ADF homology domain. In the absence of x-ray or cryo-EM structure of twinfilin-bound filament barbed ends, the mechanism of twinfilin-mediated depolymerization is less settled. Two separate modes of binding have been proposed. Twinfilin can either bind both the terminal and the penultimate actin subunits via its two ADF homology domains [51] or bind to only one of the two subunits at the barbed ends [29]. In the former configuration, twinfilin's presence would sterically hinder profilin's association to both terminal actin subunits. In the latter configuration, one of the ADF homology domains of twinfilin would interact with either the terminal or the penultimate subunit and the second ADF/cofilin domain would interact with the side of the actin filament [29]. In this scheme, the barbed end subunit not bound to twinfilin will still be able to interact with profilin. Based on these two alternative proposals, we developed kinetic models that made specific predictions about the observed depolymerization rate as a function of profilin and twinfilin concentration. Our experimental results favor the first proposal over the second; i.e., twinfilin associates with both the barbed end subunits. Taken together, twinfilin's presence at the filament barbed end prevents profilin's interactions with both barbed end subunits. Importantly, we note that these results also demonstrate the power of our theory-experiment approach—using profilin as a probe, our analysis has provided novel insights into twinfilin's binding to and depolymerization of barbed ends.

Since twinfilin and cofilin both contain ADF/cofilin homology domains, we hypothesized that these proteins would bind filament barbed ends in a mutually exclusive manner. However, to our surprise, we found that the depolymerization dynamics for these two proteins could not be explained by our simple single-site competitive binding model. Specifically, we found that experimentally measured depolymerization rates in the simultaneous presence of cofilin and twinfilin were always much slower than predicted by the model. What might explain this? Cofilin readily decorates the sides of ADP filaments. At saturating concentrations, complete side decoration of actin filaments by cofilin leads to a tenfold reduction in barbed end depolymerization compared to bare actin filaments [31,53]. However, we did not see a reduction in the depolymerization rate of ADP-P_i filaments even at high cofilin concentrations, suggesting that cofilin alone might not stably decorate the sides of actin filaments. We therefore wondered if the presence of twinfilin at the barbed end could stabilize weak interactions of cofilin with the sides of ADP-Pi actin filaments. Indeed, our revised competitive model which included cofilin side binding and its cooperative interactions with barbed-end bound twinfilin captured experimentally observed depolymerization rates. For the sake of simplicity, our model assumes that cofilin's side binding has no impact on depolymerization in the absence of twinfilin at the barbed end. A relaxation of this assumption will make the model more complex and less interpretable. Experimentally, it is extremely challenging to determine whether cofilin-mediated barbed end stabilization requires cofilin's side binding only to the terminal actin subunits or to a much larger stretch of the actin filament. Our analysis suggests that, in the presence of twinfilin, cofilin's association to only the last two barbed end subunits might be sufficient to dramatically reduce barbed end depolymerization [Fig. 6(d)]. While we cannot exclude alternative mechanisms that might also be able to explain the experimental data, our analysis shows that our model captures the experimental observations extremely well. Moreover, the binding of twinfiiln and cofilin at the barbed end is reminiscent of formation of a ternary complex between twinfilin, G-actin, and cofilin at high cofilin concentrations reported by a previous study [43]. In future, quantitative multicolor single-molecule imaging experiments will be needed to directly visualize interactions of cofilin and twinfilin at or near barbed ends, and shed light on their barbed end interplay.

After deciphering principles that govern two-protein interactions, we asked if these pairwise interactions are sufficient to describe the dynamics of the system when all three proteins are simultaneously present. To this end, we constructed a model for three-protein case explicitly incorporating the three sets of pairwise interactions. This model made specific predictions for how the average depolymerization rates would change as we tuned the concentration of one of the proteins while we kept the other two fixed. In this case, pairwise interactions were sufficient to explain our results from three-protein experiments, indicating an absence of higher-order interactions in this system unlike in other complex systems

where higher-order interactions play a significant role in dictating multicomponent interactions [58,59].

Do the depolymerization mechanisms uncovered have *in vivo* relevance? Two questions come up. First, filaments at the leading edge exhibit lifetimes of only a few seconds [60], which is about two orders of magnitude faster than timescales of P_i release ($0.002\,s^{-1}$) [54,61]. This discrepancy suggests that it is possible that filaments *in vivo* might entirely bypass the phosphate release step and get depolymerized in their ADP-P_i state, possibly by multicomponent mechanisms described here. Second, while the experiments in this study were conducted in the absence of actin monomers, cytoplasm is thought to contain up to 100 μM monomeric actin, mostly bound to either profilin or thymosin $\beta 4$. As a result, the availability of free profilin in the cytosol remains unclear. Thus, because of the high amounts of profilin-actin present in living cells, the extent to which the mechanisms uncovered here impact actin dynamics in cells is an open question.

Although we have assumed our system to be in thermodynamic equilibrium, we cannot explicitly rule out the presence of nonequilibrium mechanisms. The assumption of equilibrium employed here is a convenient way to describe the problem of multicomponent depolymerization since such a description involves only a small number of parameters. In contrast, although a nonequilibrium kinetic model might provide a more comprehensive and complete description, it requires *a priori* knowledge of the full reaction network and a higher number of parameters, which might not necessarily be available. Thus, the equilibrium thermodynamic models used here allow us to comprehend our data by taking into account only the essential ingredients. Moreover, owing to the simplicity of our modeling framework, deviations from our model could even facilitiate the discovery of nonequilibrium effects [62,63].

In summary, we implemented a bottom-up approach that builds on single-protein measurements to shed light on emergent multiprotein behavior. Single-protein measurements allow for the extraction of various rate constants, which can be utilized to build predictive models of multiprotein regulation of actin dynamics. These models can be falsified through a rigorous comparison of their predictions with experimental data. While we used this approach to shed new light on actin depolymerization by profilin, cofilin, and twinfilin, we believe this approach should be generally applicable to decipher how living cells integrate activities of multiple proteins to regulate complex intracellular actin dynamics.

IV. METHODS

A. Purification and labeling of actin

Rabbit skeletal muscle actin was purified from acetone powder generated from frozen ground hind leg muscle tissue of young rabbits (PelFreez, USA). Lyophilized acetone powder stored at −80 °C was mechanically sheared in a coffee grinder, resuspended in G-buffer (5 mM Tris-HCl pH 7.5, 0.5 mM Dithiothreitol (DTT), 0.2 mM ATP, and 0.1 mM $CaCl_2$), and cleared by centrifugation for 20 min at 50000*g*. Supernatant was collected and further filtered with Whatman paper. Actin was then polymerized overnight at 4 °C, slowly stirred, by the addition of 2 mM $MgCl_2$ and 50 mM NaCl to the filtrate. The next morning, NaCl powder was added to a final concentration of 0.6 M and stirring was continued for another 30 min at 4 °C. Then, F-actin was pelleted by centrifugation for 150 min at 280 000*g*, the pellet was solubilized by dounce homogenization and dialyzed against G-buffer for 48 h at 4 °C. Monomeric actin was then precleared at 435 000*g* and loaded onto a Sephacryl S-200 16/60 gel-filtration column (Cytiva, USA) equilibrated in G-buffer. Fractions containing actin were stored at 4 °C.

To fluorescently label actin, G-actin was polymerized by dialyzing overnight against modified F-buffer (20 mM PIPES pH 6.9, 0.2 mM $CaCl_2$, 0.2 mM ATP, 100 mM KCl) [25]. F-actin was incubated for 2 h at room temperature with a fivefold molar excess of Alexa-488 NHS ester dye (Thermo Fisher Scientific, USA). F-actin was then pelleted by centrifugation at 450 000*g* for 40 min at room temperature, and the pellet was resuspended in G-buffer, homogenized with a dounce, and incubated on ice for 2 h to depolymerize the filaments. The monomeric actin was then repolymerized on ice for 1 h by addition of 100 mM KCl and 1 mM $MgCl_2$. F-actin was once again pelleted by centrifugation for 40 min at 450 000*g* at 4 °C. The pellet was homogenized with a dounce and dialyzed overnight at 4 °C against 1 L of G-buffer. The solution was precleared by centrifugation at 450 000*g* for 40 min at 4 °C. The supernatant was collected, and the concentration and labeling efficiency of actin was determined.

B. Purification of twinfilin

Mouse mTwf1 was expressed in *Escherichia coli* BL21 (pRare). Cells were grown in Terrific Broth to log phase at 37 °C. Expression was induced overnight at 18 °C by addition of 1 mM IPTG. Cells were harvested by centrifugation at 11200*g* for 15 min and the cell pellets were stored at −80 °C. For purification, frozen pellets were thawed and resuspended in 35 mL lysis buffer (50 mM sodium phosphate buffer pH 8, 20 mM imidazole, 300 mM NaCl, 1 mM DTT, 1 mM PMSF, and protease inhibitors (pepstatin A, antipain, leupeptin, aprotinin, and chymostatin, 0.5 μM each)). Cells were lysed using a tip sonicator while kept on ice. The cell lysate was then centrifuged at 120 000*g* for 45 min at 4 °C. The supernatant was then incubated with 1 mL of Ni-NTA beads (Qiagen, USA) while rotating for 2 h at 4 °C. The beads were then washed three times with the wash buffer (50 mM sodium phosphate buffer pH 8, 300 mM NaCl, 20 mM imidazole, and 1 mM DTT). The beads were then transferred to a disposable column (Bio-Rad, USA). Protein was eluted using the elution buffer (50 mM phosphate buffer pH 8, 300 mM NaCl, 250 mM imidazole, and 1 mM DTT). Fractions containing the protein were concentrated and loaded onto a size exclusion Superdex 75 Increase 10/300 column (Cytiva, USA) preequilibrated with 20 mM HEPES pH 7.5, 1 mM EDTA, 50 mM KCl, and 1 mM DTT. Peak fractions were collected, concentrated, aliquoted, and flash-frozen in liquid N_2 and stored at −80 °C.

C. Purification of profilin

Human profilin-1 was expressed in *E. coli* strain BL21 (pRare) to log phase in LB broth at 37 °C and induced with

1 mM IPTG for 3 h at 37 °C. Cells were then harvested by centrifugation at 15000*g* at 4 °C and stored at −80 °C. For purification, pellets were thawed and resuspended in 30 mL lysis buffer (50 mM Tris-HCl pH 8, 1 mM DTT, 1 mM PMSF protease inhibitors (0.5 μM each of pepstatin A, antipain, leupeptin, aprotinin, and chymostatin)), and the solution was sonicated on ice by a tip sonicator. The lysate was centrifuged for 45 min at 120 000*g* at 4 °C. The supernatant was then passed over 20 ml of Poly-L-proline conjugated beads in a disposable column (Bio-Rad, USA). The beads were first washed at room temperature in wash buffer (10 mM Tris pH 8, 150 mM NaCl, 1 mM EDTA, and 1 mM DTT) and then washed again with two column volumes of 10 mM Tris pH 8, 150 mM NaCl, 1 mM EDTA, 1 mM DTT, and 3 M urea. Protein was then eluted with five column volumes of 10 mM Tris pH 8, 150 mM NaCl, 1 mM EDTA, 1 mM DTT, and 8 M urea. Pooled and concentrated fractions were then dialyzed in 4 L of 2 mM Tris pH 8, 0.2 mM EGTA, 1 mM DTT, and 0.01% NaN_3 (dialysis buffer) for 4 h at 4 °C. The dialysis buffer was replaced with fresh 4 L buffer and the dialysis was continued overnight at 4 °C. The protein was centrifuged for 45 min at 450 000*g* at 4 °C, concentrated, aliquoted, and flash-frozen in liquid N_2 and stored at −80 °C.

D. Purification of wild-type and mutant cofilin-1

Wild-type and mutant human cofilin-1 were expressed in *E.coli* BL21 DE3 cells. Cells were grown in Terrific Broth to log phase at 37 °C, and then expression was induced overnight at 18 °C by addition of 1 mM IPTG. Cells were collected by centrifugation and pellets were stored at −80 °C. Frozen pellets were thawed and resuspended in lysis buffer (20 mM Tris pH 8.0, 50 mM NaCl, 1 mM DTT, and protease inhibitors (0.5 μM each of pepstatin A, antipain, leupeptin, aprotinin, and chymostatin)). Cells were lysed with a tip sonicator while being kept on ice. The cell lysate was centrifuged at 150 000*g* for 30 min at 4 °C. The supernatant was loaded on a 1 mL HisTrap HP Q column (GE Healthcare, Pittsburgh, PA), and the flow-through was collected and dialyzed against 20 mM HEPES pH 6.8, 25 mM NaCl, and 1 mM DTT. The dialyzed solution was then loaded on a 1 mL HisTrap SP FF column (GE Healthcare, Pittsburgh, PA) and eluted using a linear gradient of NaCl (20–500 mM). Fractions containing protein were concentrated, dialyzed against 20 mM Tris pH 8.0, 50 mM KCl, and 1 mM DTT, and flash-frozen in liquid N_2 and stored at −80 °C.

E. Microfluidics-assisted TIRF microscopy

Actin filaments were first assembled in microfluidics-assisted TIRF (mf-TIRF) flow cells [25]. For all experiments, coverslips were first cleaned by sonication in Micro90 detergent for 20 min, followed by successive 20 min sonications in 1 M KOH, 1 M HCl, and 200 proof ethanol for 20 min each. Washed coverslips were then stored in fresh 200 proof ethanol. Coverslips were then washed extensively with H_2O and dried in an N_2 stream. These dried coverslips were coated with 2 mg/mL methoxy-poly (ethylene glycol) (mPEG)-silane, molecular weight (MW) 2000, and 2 μg/mL biotin-PEG-silane, MW 3400 (Laysan Bio, USA) in 80% ethanol (pH 2.0) and incubated overnight at 70 °C. A 40-μm-high PDMS mold with three inlets and one outlet was mechanically clamped onto a PEG-silane coated coverslip. The chamber was then connected to a Maesflo microfluidic flow-control system (Fluigent, France), rinsed with modified TIRF buffer (regular TIRF buffer supplemented with 50 mM inorganic phosphate: 10 mM imidazole pH 7.4, 34.8 mM K_2HPO_4 and 15.2 mM KH_2PO_4, 1 mM $MgCl_2$, 1 mM EGTA, 0.2 mM ATP, 10 mM DTT, and 1 mM DABCO) and incubated with 1% BSA and 10 μg/mL streptavidin in 20 mM HEPES pH 7.5, and 50 mM KCl for 5 min. The presence of 50 mM Pi in the TIRF buffer ensures that filaments remain in the ADP-P_i state throughout the experiment. Biotin spectrin-actin seeds were attached on the glass coverslip. Actin filaments with free barbed ends were then elongated by exposing the spectrin-actin seeds to a flow containing 1 μM G-actin (15% Alexa-488 labeled) and 4 μM profilin. These filaments were then exposed to profilin, cofilin, and twinfilin (alone or together) in modified-TIRF buffer. Barbed end depolymerization of these filaments was monitored. All experiments were conducted at room temperature and under continuous flow which was maintained throughout the experiment. The flow rate had no noticeable effect on depolymerization rates (see Fig. 7 of the Supplemental Material [49]).

F. Image acquisition and analysis

Single-wavelength time-lapse TIRF imaging was performed on a Nikon-Ti2000 inverted microscope equipped with a 40 mW 488 nm Argon laser, a 60× TIRF objective with a numerical aperture of 1.49 (Nikon Instruments Inc., USA), and an IXON LIFE 888 EMCCD camera (Andor Ixon, UK). One pixel was equivalent to 144 × 144 nm. Focus was maintained by the Perfect Focus system (Nikon Instruments Inc., Japan). Time-lapsed images were acquired every 10 s using Nikon Elements imaging software (Nikon Instruments Inc., Japan).

Images were analyzed in FIJI [64]. Background subtraction was conducted using the rolling ball background subtraction algorithm (ball radius 5 pixels). For each condition, between 50 and 100 filaments were acquired across multiple fields of view. To determine the rate of depolymerization, the in-built kymograph plugin was used to draw kymographs of individual filaments. The kymograph slope was used to calculate barbed end depolymerization rate of each individual filament (assuming one actin subunit contributes 2.7 nm to filament length). Data analysis and curve fitting were carried out in Microcal Origin. All experiments were repeated three times and yielded similar results. Data shown are from one trial. The predictions for the models were calculated using custom-written code in *Matlab*.

ACKNOWLEDGMENTS

We thank Heidi Ulrichs and Ekram Towsif for help with protein purification. We thank Pekka Lappalainen for critical feedback on the manuscript. S.C. is supported by the Ramalingaswami Re-entry Fellowship (BT/HRD/35/02/2006) from the Department of Biotechnology, Government of India. S.S. is supported by NIH NIGMS Grant No. R35GM143050.

[1] P. Lappalainen, T. Kotila, A. Jegou, and G. Romet-Lemonne, Biochemical and mechanical regulation of actin dynamics, Nat. Rev. Mol. Cell Biol. **23**, 836 (2022).

[2] L. Blanchoin, R. Boujemaa-Paterski, C. Sykes, and J. Plastino, Actin dynamics, architecture, and mechanics in cell motility, Physiol. Rev. **94**, 235 (2014).

[3] M. F. Carlier and S. Shekhar, Global treadmilling coordinates actin turnover and controls the size of actin networks, Nat. Rev. Mol. Cell Biol. **18**, 389 (2017).

[4] S. Shekhar, J. Pernier, and M. F. Carlier, Regulators of actin filament barbed ends at a glance, J. Cell Sci. **129**, 1085 (2016).

[5] B. L. Goode, J. Eskin, and S. Shekhar, Mechanisms of actin disassembly and turnover, J. Cell Biol. **222**, e202309021 (2023).

[6] T. Kouyama and K. Mihashi, Fluorimetry study of N-(1-pyrenyl)iodoacetamide-labelled F-actin. Local structural change of actin protomer both on polymerization and on binding of heavy meromyosin, Eur. J. Biochem. **114**, 33 (1981).

[7] B. A. Smith, K. Daugherty-Clarke, B. L. Goode, and J. Gelles, Pathway of actin filament branch formation by Arp2/3 complex revealed by single-molecule imaging, Proc. Natl. Acad. Sci. USA **110**, 1285 (2013).

[8] B. A. Smith, S. B. Padrick, L. K. Doolittle, K. Daugherty-Clarke, I. R. Correa, Jr., M. Q. Xu, B. L. Goode, M. K. Rosen, and J. Gelles, Three-color single molecule imaging shows WASP detachment from Arp2/3 complex triggers actin filament branch formation, eLife **2**, e01008 (2013).

[9] D. Breitsprecher, R. Jaiswal, J. P. Bombardier, C. J. Gould, J. Gelles, and B. L. Goode, Rocket launcher mechanism of collaborative actin assembly defined by single-molecule imaging, Science **336**, 1164 (2012).

[10] S. Shekhar, M. Kerleau, S. Kuhn, J. Pernier, G. Romet-Lemonne, A. Jegou, and M. F. Carlier, Formin and capping protein together embrace the actin filament in a menage a trois, Nat. Commun. **6**, 8730 (2015).

[11] J. P. Bombardier, J. A. Eskin, R. Jaiswal, I. R. Correa, Jr., M. Q. Xu, B. L. Goode, and J. Gelles, Single-molecule visualization of a formin-capping protein "decision complex" at the actin filament barbed end, Nat. Commun. **6**, 8707 (2015).

[12] H. Ulrichs, I. Gaska, and S. Shekhar, Multicomponent regulation of actin barbed end assembly by twinfilin, formin and capping protein, Nat. Commun. **14**, 3981 (2023).

[13] E. M. Towsif and S. Shekhar, Cyclase-associated protein is a pro-formin anti-capping processive depolymerase of actin barbed and pointed ends, bioRxiv (2023).

[14] S. Shekhar, J. Chung, J. Kondev, J. Gelles, and B. L. Goode, Synergy between cyclase-associated protein and cofilin accelerates actin filament depolymerization by two orders of magnitude, Nat. Commun. **10**, 5319 (2019).

[15] T. Kotila, H. Wioland, G. Enkavi, K. Kogan, I. Vattulainen, A. Jegou, G. Romet-Lemonne, and P. Lappalainen, Mechanism of synergistic actin filament pointed end depolymerization by cyclase-associated protein and cofilin, Nat. Commun. **10**, 5320 (2019).

[16] E. M. Towsif, B. A. Miller, H. Ulrichs, and S. Shekhar, Multicomponent depolymerization of actin filament pointed ends by cofilin and cyclase-associated protein depends upon filament age, Eur. J. Cell Biol. **103**, 151423 (2024).

[17] J. Pernier, J. Orban, B. S. Avvaru, A. Jegou, G. Romet-Lemonne, B. Guichard, and M. F. Carlier, Dimeric WH2 domains in *Vibrio* VopF promote actin filament barbed-end uncapping and assisted elongation, Nat. Struct. Mol. Biol. **20**, 1069 (2013).

[18] N. Courtemanche and T. D. Pollard, Interaction of profilin with the barbed end of actin filaments, Biochemistry **52**, 6456 (2013).

[19] J. Funk, F. Merino, M. Schaks, K. Rottner, S. Raunser, and P. Bieling, A barbed end interference mechanism reveals how capping protein promotes nucleation in branched actin networks, Nat. Commun. **12**, 5329 (2021).

[20] P. J. Carman, K. R. Barrie, G. Rebowski, and R. Dominguez, Structures of the free and capped ends of the actin filament, Science **380**, 1287 (2023).

[21] K. J. Amann and T. D. Pollard, Direct real-time observation of actin filament branching mediated by Arp2/3 complex using total internal reflection fluorescence microscopy, Proc. Natl. Acad. Sci. USA **98**, 15009 (2001).

[22] J. R. Kuhn and T. D. Pollard, Real-time measurements of actin filament polymerization by total internal reflection fluorescence microscopy, Biophys. J. **88**, 1387 (2005).

[23] S. K. Maciver, H. G. Zot, and T. D. Pollard, Characterization of actin filament severing by actophorin from *Acanthamoeba castellanii*, J. Cell Biol. **115**, 1611 (1991).

[24] A. Jegou, T. Niedermayer, J. Orban, D. Didry, R. Lipowsky, M. F. Carlier, and G. Romet-Lemonne, Individual actin filaments in a microfluidic flow reveal the mechanism of ATP hydrolysis and give insight into the properties of profilin, PLoS Biol. **9**, e1001161 (2011).

[25] S. Shekhar, Microfluidics-assisted TIRF imaging to study single actin filament dynamics, Curr. Protoc. Cell Biol. **77**, 12.13.1 (2017).

[26] S. Shekhar, G. J. Hoeprich, J. Gelles, and B. L. Goode, Twinfilin bypasses assembly conditions and actin filament aging to drive barbed end depolymerization, J. Cell Biol. **220** e202006022 (2021).

[27] S. Shekhar and M. F. Carlier, Enhanced depolymerization of actin filaments by ADF/cofilin and monomer funneling by capping protein cooperate to accelerate barbed-end growth, Curr. Biol. **27**, 1990 (2017).

[28] J. Pernier, S. Shekhar, A. Jegou, B. Guichard, and M. F. Carlier, Profilin interaction with actin filament barbed end controls dynamic instability, capping, branching, and motility, Dev. Cell **36**, 201 (2016).

[29] M. Hakala, H. Wioland, M. Tolonen, T. Kotila, A. Jegou, G. Romet-Lemonne, and P. Lappalainen, Twinfilin uncaps filament barbed ends to promote turnover of lamellipodial actin networks, Nat. Cell Biol. **23**, 147 (2021).

[30] L. Cao, M. Kerleau, E. L. Suzuki, H. Wioland, S. Jouet, B. Guichard, M. Lenz, G. Romet-Lemonne, and A. Jegou, Modulation of formin processivity by profilin and mechanical tension, eLife **7** e34176 (2018).

[31] H. Wioland, B. Guichard, Y. Senju, S. Myram, P. Lappalainen, A. Jegou, and G. Romet-Lemonne, ADF/cofilin accelerates actin dynamics by severing filaments and promoting their depolymerization at both ends, Curr. Biol. **27**, 1956 (2017).

[32] S. Shekhar and M. F. Carlier, Single-filament kinetic studies provide novel insights into regulation of actin-based motility, Mol. Biol. Cell **27**, 1 (2016).

[33] M. F. Carlier, Measurement of P_i dissociation from actin filaments following ATP hydrolysis using a linked enzyme assay, Biochem. Biophys. Res. Commun. **143**, 1069 (1987).

[34] M. F. Carlier and D. Pantaloni, Direct evidence for ADP-P_i-F-actin as the major intermediate in ATP-actin polymerization. Rate of dissociation of P_i from actin filaments, Biochemistry **25**, 7789 (1986).

[35] L. Carlsson, L. E. Nystrom, I. Sundkvist, F. Markey, and U. Lindberg, Actin polymerizability is influenced by profilin, a low molecular weight protein in non-muscle cells, J. Mol. Biol. **115**, 465 (1977).

[36] F. Markey, H. Larsson, K. Weber, and U. Lindberg, Nucleation of actin polymerization from profilactin. Opposite effects of different nuclei, Biochim. Biophys. Acta **704**, 43 (1982).

[37] D. Pantaloni and M. F. Carlier, How profilin promotes actin filament assembly in the presence of thymosin beta 4, Cell **75**, 1007 (1993).

[38] H. J. Kinosian, L. A. Selden, L. C. Gershman, and J. E. Estes, Actin filament barbed end elongation with nonmuscle MgATP-actin and MgADP-actin in the presence of profilin, Biochemistry **41**, 6734 (2002).

[39] S. Romero, C. Le Clainche, D. Didry, C. Egile, D. Pantaloni, and M. F. Carlier, Formin is a processive motor that requires profilin to accelerate actin assembly and associated ATP hydrolysis, Cell **119**, 419 (2004).

[40] S. M. Ahern-Djamali, C. Bachmann, P. Hua, S. K. Reddy, A. S. Kastenmeier, U. Walter, and F. M. Hoffmann, Identification of profilin and src homology 3 domains as binding partners for *Drosophila* Enabled, Proc. Natl. Acad. Sci. USA **96**, 4977 (1999).

[41] D. Breitsprecher, A. K. Kiesewetter, J. Linkner, M. Vinzenz, T. E. Stradal, J. V. Small, U. Curth, R. B. Dickinson, and J. Faix, Molecular mechanism of Ena/VASP-mediated actin-filament elongation, EMBO J. **30**, 456 (2011).

[42] M. F. Carlier, V. Laurent, J. Santolini, R. Melki, D. Didry, G. X. Xia, Y. Hong, N. H. Chua, and D. Pantaloni, Actin depolymerizing factor (ADF/cofilin) enhances the rate of filament turnover: Implication in actin-based motility, J. Cell Biol. **136**, 1307 (1997).

[43] P. J. Ojala, V. O. Paavilainen, M. K. Vartiainen, R. Tuma, A. G. Weeds, and P. Lappalainen, The two ADF-H domains of twinfilin play functionally distinct roles in interactions with actin monomers, Mol. Biol. Cell **13**, 3811 (2002).

[44] M. Vartiainen, P. J. Ojala, P. Auvinen, J. Peranen, and P. Lappalainen, Mouse A6/twinfilin is an actin monomer-binding protein that localizes to the regions of rapid actin dynamics, Mol. Cell. Biol. **20**, 1772 (2000).

[45] B. L. Goode, D. G. Drubin, and P. Lappalainen, Regulation of the cortical actin cytoskeleton in budding yeast by twinfilin, a ubiquitous actin monomer-sequestering protein, J. Cell Biol. **142**, 723 (1998).

[46] V. O. Paavilainen, E. Oksanen, A. Goldman, and P. Lappalainen, Structure of the actin-depolymerizing factor homology domain in complex with actin, J. Cell Biol. **182**, 51 (2008).

[47] L. Blanchoin and T. D. Pollard, Interaction of actin monomers with *Acanthamoeba* actophorin (ADF/cofilin) and profilin, J. Biol. Chem. **273**, 25106 (1998).

[48] C. E. Schutt, J. C. Myslik, M. D. Rozycki, N. C. Goonesekere, and U. Lindberg, The structure of crystalline profilin-beta-actin, Nature (London) **365**, 810 (1993).

[49] See Supplemental Material at http://link.aps.org/supplemental/10.1103/PRXLife.2.033002 for Supplemental Figs. 1–10 and detailed description of mathematical methods developed in this manuscript.

[50] R. Phillips, J. Kondev, J. Theriot, and H. Garcia, *Physical Biology of the Cell*, 2nd ed. (Garland Science, London, 2012).

[51] D. M. Mwangangi, E. Manser, and R. C. Robinson, The structure of the actin filament uncapping complex mediated by twinfilin, Sci. Adv. **7** eabd5271 (2021).

[52] R. Kardos, K. Pozsonyi, E. Nevalainen, P. Lappalainen, M. Nyitrai, and G. Hild, The effects of ADF/cofilin and profilin on the conformation of the ATP-binding cleft of monomeric actin, Biophys. J. **96**, 2335 (2009).

[53] C. Suarez *et al.*, Cofilin tunes the nucleotide state of actin filaments and severs at bare and decorated segment boundaries, Curr. Biol. **21**, 862 (2011).

[54] L. Blanchoin and T. D. Pollard, Mechanism of interaction of *Acanthamoeba* actophorin (ADF/cofilin) with actin filaments, J. Biol. Chem. **274**, 15538 (1999).

[55] K. Hayakawa, S. Sakakibara, M. Sokabe, and H. Tatsumi, Single-molecule imaging and kinetic analysis of cooperative cofilin-actin filament interactions, Proc. Natl Acad. Sci. USA **111**, 9810 (2014).

[56] P. Lappalainen, E. V. Fedorov, A. A. Fedorov, S. C. Almo, and D. G. Drubin, Essential functions and actin-binding surfaces of yeast cofilin revealed by systematic mutagenesis, EMBO J. **16**, 5520 (1997).

[57] W. Oosterheert, B. U. Klink, A. Belyy, S. Pospich, and S. Raunser, Structural basis of actin filament assembly and aging, Nature (London) **611**, 374 (2022).

[58] F. Battiston *et al.*, The physics of higher-order interactions in complex systems, Nat. Phys. **17**, 1093 (2021).

[59] A. Sanchez-Gorostiaga, D. Bajic, M. L. Osborne, J. F. Poyatos, and A. Sanchez, High-order interactions distort the functional landscape of microbial consortia, PLoS Biol. **17**, e3000550 (2019).

[60] N. Watanabe and T. J. Mitchison, Single-molecule speckle analysis of actin filament turnover in lamellipodia, Science **295**, 1083 (2002).

[61] R. Melki, S. Fievez, and M. F. Carlier, Continuous monitoring of P_i release following nucleotide hydrolysis in actin or tubulin assembly using 2-amino-6-mercapto-7-methylpurine ribonucleoside and purine-nucleoside phosphorylase as an enzyme-linked assay, Biochemistry **35**, 12038 (1996).

[62] M. Morrison, M. Razo-Mejia, and R. Phillips, Reconciling kinetic and thermodynamic models of bacterial transcription, PLoS Comput. Biol. **17**, e1008572 (2021).

[63] J. Estrada, F. Wong, A. DePace, and J. Gunawardena, Information integration and energy expenditure in gene regulation, Cell **166**, 234 (2016).

[64] J. Schindelin *et al.*, Fiji: An open-source platform for biological-image analysis, Nat. Methods **9**, 676 (2012).